# Dynamic Constitutive and Failure Behavior of a Two-Phase Tungsten Composite

**M. Zhou**
George W. Woodruff School of Mechanical Engineering, Georgia Institute of Technology, Atlanta, GA 30332-0405
Assoc. Mem. ASME

**R. J. Clifton**
Division of Engineering, Brown University, Providence, RI 02912
Mem. ASME.

*The constitutive response and failure behavior of a W-Ni-Fe alloy over the strain rate range of $10^{-4}$ to $5 \times 10^{5}$ $s^{-1}$ is experimentally investigated. Experiments conducted are pressure-shear plate impact, torsional Kolsky bar, and quasi-static torsion. The material has a microstructure of hard tungsten grains embedded in a soft alloy matrix. Nominal shear stress-strain relations are obtained for deformations throughout the experiments and until after the initiation of localization. Shear bands form when the plastic strain becomes sufficiently large, involving both the grains and the matrix. The critical shear strain for shear band development under the high rate, high pressure conditions of pressure-shear is approximately 1–1.5 or 6–8 times that obtained in torsional Kolsky bar experiments which involve lower strain rates and zero pressure. Shear bands observed in the impact experiments show significantly more intensely localized deformation. Eventual failure through the shear band is a combination of grain-matrix separation, ductile matrix rupture, and grain fracture. In order to understand the effect of the composite microstructure and material inhomogeneity on deformation, two other materials are also used in the study. One is a pure tungsten and the other is an alloy of W, Ni, and Fe with the same composition as that of the matrix phase in the overall composite. The results show that the overall two-phase composite is more susceptible to the formation of shear bands than either of its constituents.*

## 1 Introduction

Tungsten heavy alloys (WHA or tungsten composites) are characterized by high density, high strength, and high toughness resulting from their composite microstructures of hard tungsten grains embedded in a ductile matrix. Because of these properties and such qualities as good machinability, low cost, and nonradioactivity, they are candidate materials for kinetic energy penetrators. Traditionally, the mechanical properties of these materials have been studied by means of tensile and compressive tests under quasi-static or low strain rate conditions, Churn et al. (1984), O'Donnell et al. (1990), Rabin et al. (1988), Krock et al. (1963), and Krock (1964). However, WHA with different properties as characterized by such tests have demonstrated similar penetrating capabilities which are worse than that of depleted Uranium (see e.g., Magness (1992)), suggesting that the behavior of these materials under impact conditions are dominated by deformation and failure mechanisms not accounted for by such material properties as tensile strengths and ductility. Magness (1992) also reported that the performance of penetrator materials depends strongly on the formation of shear bands. Specifically, the localization of plastic deformation associated with the development of shear bands and the eventual material failure significantly improve the performance of these penetrators by allowing deformed materials to be discarded. Zurek et al. (1995) compared the behavior of a tungsten composite with that of a depleted Uranium over the strain rate range of $10^{-3}$ to 6000 $s^{-1}$ and suggested that the enhanced susceptibility to shear localization of the Uranium is due to the existence of a soft high-temperature phase. Indeed, the dynamic process involves material deformation at high strain rates and high hydrostatic pressures. Under such conditions, more deformation and failure mechanisms are operative than those found in the quasi-static tests, including rate sensitivity, thermal softening, and the effect of inertia.

Investigations have indicated that WHA demonstrate significant rate sensitivity between low and moderate strain rates. Woodward et al. (1985) studied the effect of strain rate on the flow stress of three WHA over the range of $10^{-3}$ to $10^{3}$ $s^{-1}$ and reported an increase of flow stress with increasing strain rate. Thermal softening was observed for strain rates greater than 2 $s^{-1}$. Coates et al. (1990a, 1990b, 1992) found a 25 percent increase in flow stress at a strain of 8 percent over the strain rate range of $10^{-4}$ to $7 \times 10^{3}$ $s^{-1}$ in alloys containing 90 percent to 97 percent W. Increasing strength and decreasing ductility with increasing strain rates in tensile and compression tests have also been reported by Meyer et al. (1983). Andrews et al. (1992) and Weerasooriya et al. (1992) studied the formation of shear bands in WHA using torsional Kolsky bar experiments. Shear bands observed under their test conditions have an average width of 50—100 $\mu$m and the critical strain at which shear bands form is approximately 0.15–0.25. Andrews et al. (1992) also found that the peak temperature in the shear bands is about 580°C and axial pressures delay the process of shear band formation. The behavior of tungsten composites at strain rates up to $8 \times 10^{4}$ $s^{-1}$ has also been analyzed by Baek et al. (1994), Belk et al. (1994), Weerasooriya (1994), Weerasooriya et al. (1994), Woodward et al. (1994), Tham et al. (1995), Yadav et al. (1995), and Zhao et al. (1995).

Higher strain rates and higher pressures exist in penetration. In order to improve the performance through revisions in material design and processing, it is necessary to characterize the material behavior under high-rate and high-pressure conditions similar to those in actual applications. This need calls for experiments that involve strain rates up to $10^{6}$ $s^{-1}$ and pressures up to 8–10 GPa. Pressure-shear plate impact, as described by Clif-

Contributed by the Applied Mechanics Division of THE AMERICAN SOCIETY OF MECHANICAL ENGINEERS for publication in the ASME JOURNAL OF APPLIED MECHANICS.

Discussion on the paper should be addressed to the Technical Editor, Professor Lewis T. Wheeler, Department of Mechanical Engineering, University of Houston, Houston, TX 77204-4792, and will be accepted until four months after final publication of the paper itself in the ASME JOURNAL OF APPLIED MECHANICS.

Manuscript received by the ASME Applied Mechanics Division, Mar. 4, 1996; final revision, Nov. 4, 1996. Associate Technical Editor: W. N. Sharpe, Jr.

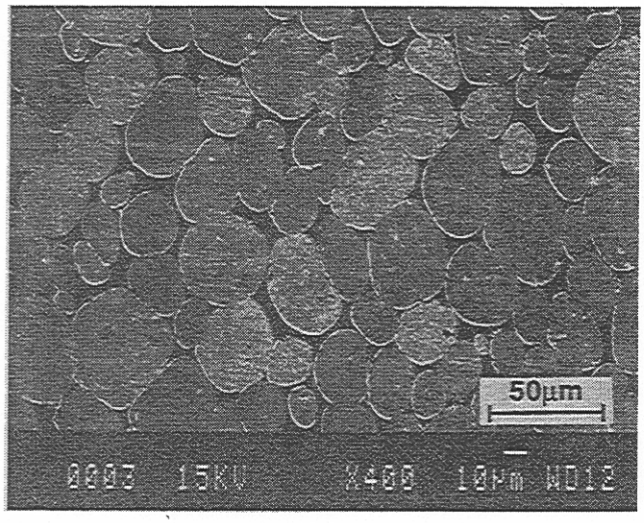


(a)

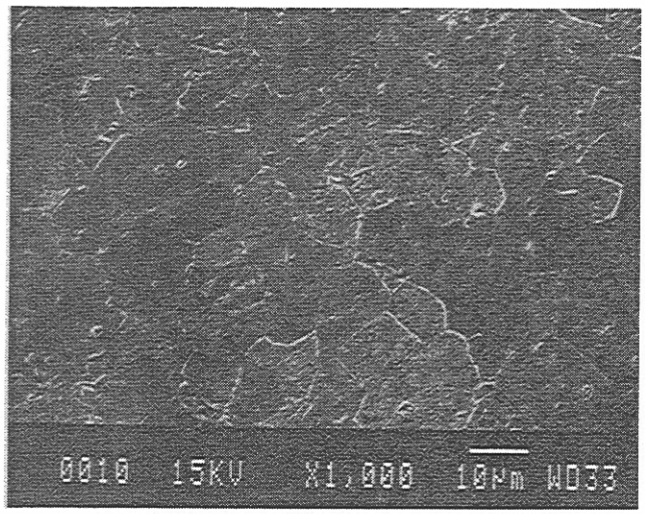


(b)

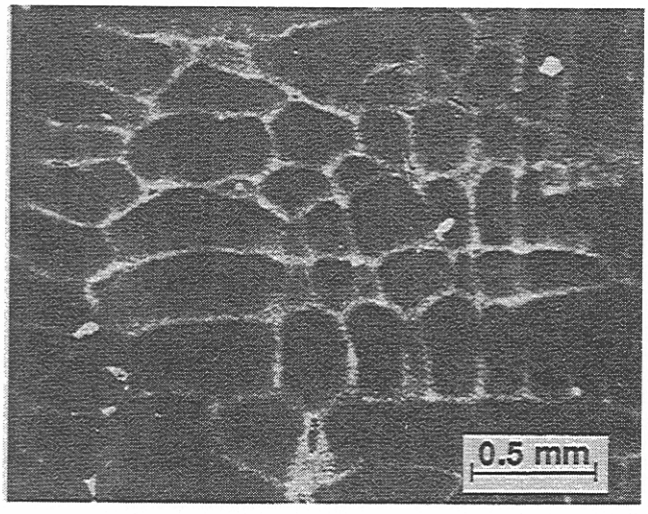


(c)

Fig. 1 Microstructures of materials used; (*a*) tungsten composite, (*b*) pure tungsten, and (*c*) matrix alloy

ton et al. (1985), provides an attractive means for achieving such strain rates and pressures under well-characterized plane-strain conditions. In this investigation, controlled shear band formation is studied using the pressure-shear configuration. In addition, constitutive responses at intermediate and quasi-static strain rates are studied using a torsional Kolsky bar apparatus. The combined pressure-shear impact, torsional Kolsky bar, and quasi-static torsion experiments allow material responses over the strain rate range of $10^{-4}$ to $10^{6}$ $s^{-1}$ to be characterized.

## 2 Materials

Figure 1(*a*) shows the microstructure of the tungsten heavy alloy used in the study. This microstructure consists of tungsten grains embedded in a matrix phase of nickel, iron, and tungsten. This material contains 93wt%–W, 4.9wt%–Ni and 2.1wt%–Fe. In order to understand the effects of the two-phase microstructure and material inhomogeneities on the behavior of the alloy, a pure tungsten and a Ni-W-Fe alloy are used to determine the responses of the two constituent phases in the composite. The matrix alloy, having a composition of 50wt%–Ni, 25wt%–Fe, and 25wt%–W, is custom made to match the the composition of the matrix phase (Ekbom, 1981; O'Donnell et al., 1990; Hofmann et al., 1984) in the composite. All materials are sintered and cross-rolled along two perpendicular directions in the rolling plane to a thickness reduction of eight percent in each direction to obtain comparable dislocation structures so that direct comparisons could be made between the response of the WHA and its constituents. The microstructures of the pure tungsten and the matrix alloy are shown in Figs. 1(*b*) and 1(*c*), respectively.

## 3 Experiments

In the pressure-shear plate impact experiment, the specimen is a disk 50 $\mu$m to 200 $\mu$m in thickness. The specimen material is subjected to simple shear for 2 $\mu$s at nominal shear strain rates between $10^{5}$ and $10^{6}$ $s^{-1}$, under pressures on the order of 8–10 GPa. Because of its well-characterized plane-strain conditions, this experiment is an excellent configuration for studying material constitutive response at very high strain rates when uniform deformation is sustained in the specimen. This experiment also allows the onset of shear localization and the development of a shear band to be interpreted from the stress-time and stress-strain profiles. Since the specimen has no free surface, shear band initiation and development are insensitive to macroscopic geometrical defects, which may significantly influence the initiation and development of shear bands in other experimental configurations, such as torsional Kolsky bar (Mol-

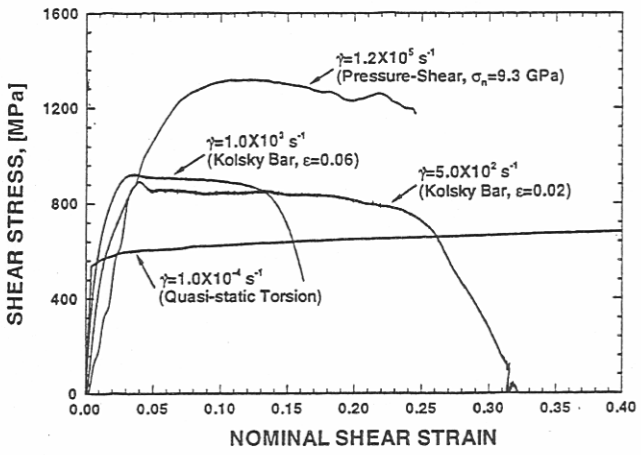


Fig. 2 Shear stress-strain curves of WHA obtained from pressure-shear plate impact, torsional Kolsky bar, and quasi-static torsion experiments

Table 1 Pressure-shear experiment on WHA, W, and matrix alloy

| Shot # | Specimen Material | Projectile Velocity mm/$\mu$s | Skew Angle ° | Normal Pressure MPa | Shear Stress MPa | Shear Rate $\times 10^5 s^{-1}$ | Specimen Thickness $\mu$m | Shear Band |
|---|---|---|---|---|---|---|---|---|
| 9109 | WHA | 0.181 | 21.5 | 8981 | 1100 | 0.14 | 1973 | No |
| 9201 | WHA | 0.188 | 22.0 | 9326 | 1300 | 1.2 | 201 | No |
| 9205 | WHA | 0.205 | 21.5 | 10689 | 1350 | 3.9 | 78 | Yes |
| 9206 | WHA | 0.202 | 26.6 | 9629 | 1300 | 5.4 | 87 | Yes |
| 9207 | WHA | 0.213 | 22.0 | 10555 | 1350 | 4.0 | 89 | Yes |
| 9209 | WHA | 0.205 | 18.0 | 10430 | 1290 | 3.5 | 61 | No |
| 9211 | WHA | 0.205 | 21.5 | 10174 | 1250 | 6.5 | 57 | Yes |
| 9303 | WHA | 0.198 | 22.9 | 9748 | 1320 | 4.2 | 79 | Yes |
| 9301 | W | 0.198 | 22.9 | 9733 | 1250 | 4.2 | 91 | No |
| 9302 | W | 0.206 | 22.9 | 10142 | 1320 | 2.5 | 151 | No |
| 9208 | Matrix | 0.200 | 18.0 | 10146 | 680 | 3.0 | 129 | No |
| 9212 | Matrix | 0.199 | 21.5 | 9910 | 780 | 9.0 | 55 | No |

inari et al., 1987). Table 1 summarizes the pressure-shear plate impact experiments conducted on the WHA, the pure tungsten, and the matrix alloy.

Torsional Kolsky bar experiments are conducted on the matrix alloy. In addition, data from similar experiments conducted by Andrews et al. (1992) on the same WHA are used in the discussions. This experiment has been described in, e.g., Hartley et al. (1985), Duffy et al. (1971), and Costin et al. (1979). Quasi-static torsion experiments are conducted on the torsional Kolsky bar apparatus with minor modifications. Table 2 summarizes the torsional Kolsky bar and quasistatic torsion experiments conducted on the matrix alloy. Tests at elevated temperatures of 200°C and 250°C were conducted to gain information on the temperature dependence of the stress-strain curves.

## 4 Experimental Results

**4.1 Shear Band Formation and Strain-Rate Effect.** Figure 2 shows the shear stress-strain curves of the WHA at different strain rates obtained by pressure-shear impact, torsional Kolsky bar, and quasi-static torsion. Over the strain rate range of $10^{-4}$ to $1.2 \times 10^5$ $s^{-1}$ shown, the flow stress level increases 2.5 times (from 570 to 1360 MPa), suggesting a strong rate sensitivity of the stress-strain relation. The alloy shows strain hardening under the quasi-static strain rate. The curves at the higher strain rates indicate strain softening of the material. This decrease in stress with increasing strain is attributed to thermal softening due to heat generated by the plastic deformation and the lack of time for the heat to be diffused out of the specimen. The precipitous drops in stress shown by the Kolsky bar curves indicate the onset of shear localization. The critical strains at which shear bands form are between 0.12–0.25. The defect parameter $\epsilon$, defined as the maximum wall thickness variation in the gauge section of the specimen divided by the average wall thickness, has a strong influence on the critical strain for shear localization. No sharp downturn in stress is seen in the curve obtained by pressure-shear impact although the overall rate of strain softening and the amount of accumulated shear strain are comparable to those in the Kolsky bar curves. This lack of quick loss of stress-carrying capability signifies that no localization has occurred, as confirmed by the deformed microstructure of the specimen (see the next section). The continuation of uniform deformation beyond the critical shear strains of the torsional experiments suggests that the formation of shear bands have been delayed under conditions of the impact experiment.

Shear localization is observed in impact experiments as the total amount of shear strain is increased by decreasing the specimen thickness and increasing impact velocity and impact angle. Figure 3 shows the stress-strain curves from three shots involving specimens 57–87 $\mu$m in thickness and impact angles of 18–26.6°. The sharp downturns in the curves of the two higher angle shots (9206 and 9211) signify the loss of stress-carrying capability associated with the onset of shear localization. The critical shear strains at the onset of localization are between 1–1.5. These values are six to eight times those obtained in the torsional Kolsky bar experiments (Fig. 2). Several factors may contribute to delaying shear band formation in pressure-shear

Table 2 Torsional experiments on matrix alloy

| Specimen # | Test Temperature °C (K) | Nominal Shear Strain Rate $s^{-1}$ | Flow Stress MPa | Defect Parameter $\epsilon$ | Shear Band |
|---|---|---|---|---|---|
| M1 | 250 (523) | $1.3 \times 10^3$ | 430 | 0.118 | No |
| M2 | 20 (293) | $0.5 \times 10^3$ | 570 | 0.147 | No |
| M3 | 200 (473) | $1.5 \times 10^3$ | 490 | 0.123 | No |
| M4 | 20 (293) | $1.4 \times 10^3$ | 580 | 0.095 | No |
| M6 | 20 (293) | $2.7 \times 10^3$ | 590 | 0.054 | No |
| M7 | 20 (293) | $2.6 \times 10^3$ | 590 | 0.062 | No |
| M8 | 250 (523) | $2.7 \times 10^3$ | 400 | 0.130 | No |
| M9 | 20 (293) | $\sim 1.0 \times 10^{-4}$ | 320 | 0.086 | No |
| M11 | 20 (293) | $\sim 1.0 \times 10^{-4}$ | 350 | 0.120 | No |

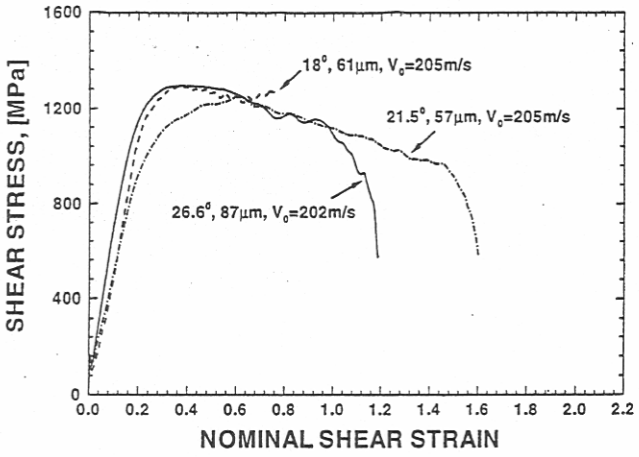


Fig. 3 Dynamic shear stress-strain curves of WHA obtained by pressure-shear plate impact

impact. Higher strain rates cause the material to flow at higher levels of stress. This increase in stress tends to stabilize the localization of deformation through higher flow stresses inside emerging shear bands where strain rates are higher. Normal pressures applied to the specimen during impact suppress the development of microvoids which would develop in the absence of pressure. This retardation reduces the additional softening caused by progressive microrupture. The normal pressure on the specimen makes the pressure-shear configuration insensitive to macroscopic geometric variations of the specimen. Such variations expedite the initiation and development of shear bands in the torsional Kolsky bar configuration (Molinari et al., 1987). Material inertia effect at high rates of deformation may also delay the development of shear bands.

**4.2 Microscopic Observations.** A series of scanning electron micrographs are obtained to show the deformation of the phases, the morphology of the shear bands, and the damage mechanisms that are responsible for eventual failure of the material inside the shear bands. The deformed microstructure of the specimen corresponding to the stress-strain curve in Fig. 2 that is obtained from pressure-shear impact is shown in Fig. 4. The elliptical grain shapes demonstrate the direction of the shear deformation. The deformation appears to be uniform across the

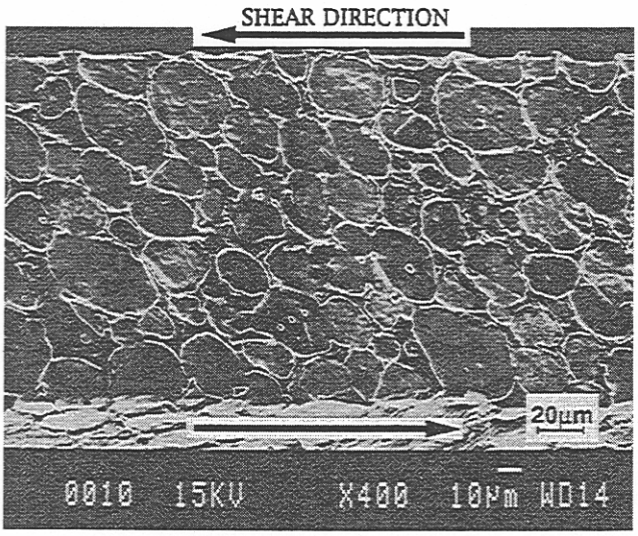


Fig. 4 Deformed microstructure of WHA after pressure-shear impact, $V_0$ = 188 ms$^{-1}$, $\theta$ = 22 deg, and $h$ = 201 $\mu$m

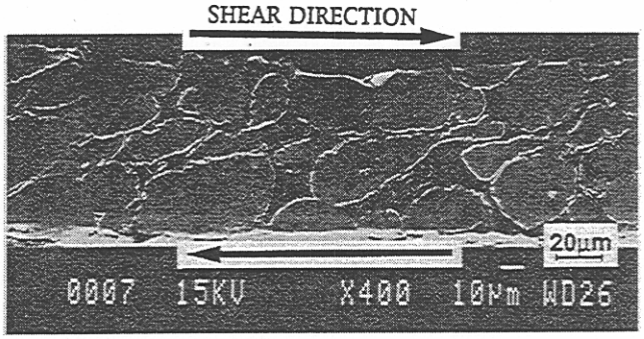


(a)

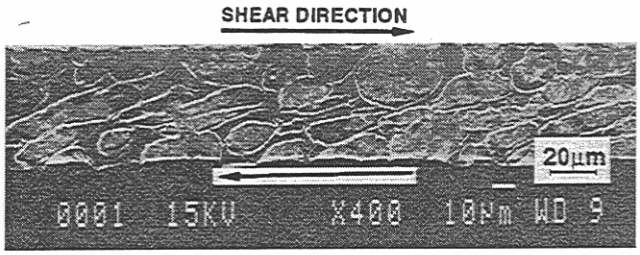


(b)

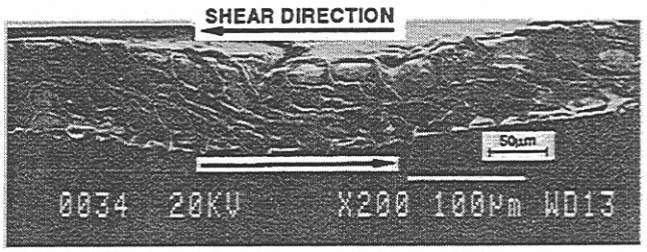


(c)

Fig. 5 Shear band morphologies in specimens after pressure-shear plate impact; (*a*) $V_0$ = 205 ms$^{-1}$, $\theta$ = 21.5 deg, and $h$ = 78 $\mu$m, sheared for 1.44 $\mu$s, (*b*) $V_0$ = 205 ms$^{-1}$, $\theta$ = 21.5 deg, and $h$ = 57 $\mu$m, sheared for 2 $\mu$s, and (*c*) $V_0$ = 202 ms$^{-1}$, $\theta$ = 26.6 deg, and $h$ = 87 $\mu$m, sheared for 2 $\mu$s

thickness and no shear band is observed. This observation is consistent with the shape of the stress-stress curve in Fig. 2 which does not show a sharp drop in stress.

Figure 5 shows shear band morphologies at different stages of development. The specimens are subjected to successively more intense shear loading. All three shots have similar impact velocities between 202–205 ms$^{-1}$ and the specimens are 57–87 $\mu$m in thickness. Figure 5(*a*) shows the deformed microstructure of a specimen sheared for approximately 1.44 $\mu$s. The micrograph shows a nucleating band at the center of the specimen. A neck has formed in the tear-drop-shaped grain. Further development of the band would involve shearing of this grain and propagation on both sides of the nucleating band. Figure 5(*b*) shows the morphology of a developing shear band in a specimen sheared for 2 $\mu$s. The impact angle and the impact velocity are the same as those for Fig. 5(*a*). Heavily elongated grains in the middle of the specimen indicate the developing

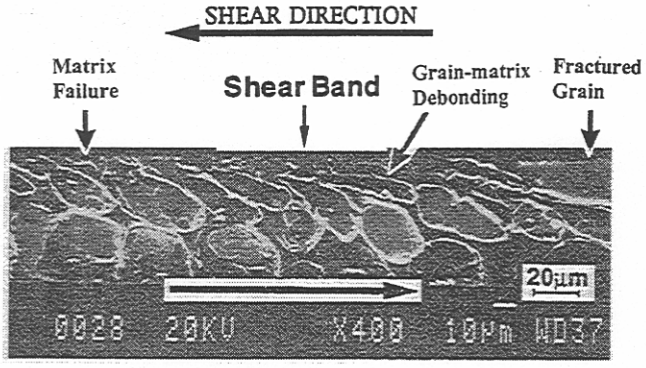


Fig. 6 A shear band that has led to fracture of a WHA specimen, $V_0$ = 213 ms$^{-1}$, $\theta$ = 22 deg, and $h$ = 89 $\mu$m

shear band. The intensely sheared region involves both the W gains and the matrix. In Fig. 5($c$), a shear band with more intensely localized deformation is seen. The micrograph shows deep etching of the grains so that the structure of the deformed matrix and grains is clearly revealed. The grains form tear-drop shapes near the middle of the band. The different distributions of deformation across the shear bands in Figs. 5($b$) and 5($c$) suggest that after the onset of shear localization further deformation occurs primarily in the center of the bands.

The shear bands in Fig. 5($b$–$c$) have widths of approximately 5–10 $\mu$m. This is in sharp contrast to the widths of approximately 100 $\mu$m reported for torsional Kolsky bar experiments (Andrews et al., 1992). Although many factors may influence the width of shear bands, heat conduction over the time duration of the experiments sets one of the length scales for the localization of deformation. In the pressure-shear impact experiment, the specimen is sheared for 2 $\mu$s. The torsional Kolsky bar experiment subjects specimens to torsional loading of up to 600 $\mu$s in duration. At higher strain rates, shear bands develop over a shorter time. Consequently, heat conduction occurs over a shorter distance. The more localized high temperatures contribute to the formation of narrower shear bands. The shear bands in Fig. 5 also show more intense shear than what has been observed in the torsional Kolsky bar experiments (see Andrews et al. (1992) and Weerasooriya et al. (1992)). Prolonged shear band development occurs in pressure-shear impact partly because high pressures (9.62 GPa and 10.17 GPa for the two specimens in Figs. 5($b$–$c$)) delay failure due to microvoids and microcracks. During the torsional Kolsky bar experiments, rupture occurs at relatively early stages of localized deformation in the absence of pressure.

The shear band in Fig. 5($c$) indicates that more intense shear deformation occurs in the matrix. Parts of the grains that are involved in the shear band form thin tails. As the deformation continues, grain-matrix separation and matrix rupture may occur due to strain incompatibility. A shear band that has led to the failure of the composite is shown in Figure 6. Note that the original thickness of this specimen is approximately twice of that shown in the picture. Only one half is shown because fracture occurred through the shear band, in the middle of the specimen. The top surface of the piece shown is the center line of the shear band through which fracture occurred. Ductile rupture of the matrix, grain-matrix separation, and grain fracture can be seen. A fractograph of the ruptured shear band surface is shown in Fig. 7. The dark areas are the matrix and the light regions are the grains. The surface morphology indicates intense shearing at the center of the shear band. Note the fractured grain at A. Dark strips on the grain surfaces indicate grain-matrix contact before separation. Because of the high percentage of the fracture surface that carries the grain-matrix shear marks, grain-matrix separation appears to be the dominant failure mechanism. A group of light grains with no dark contact marks

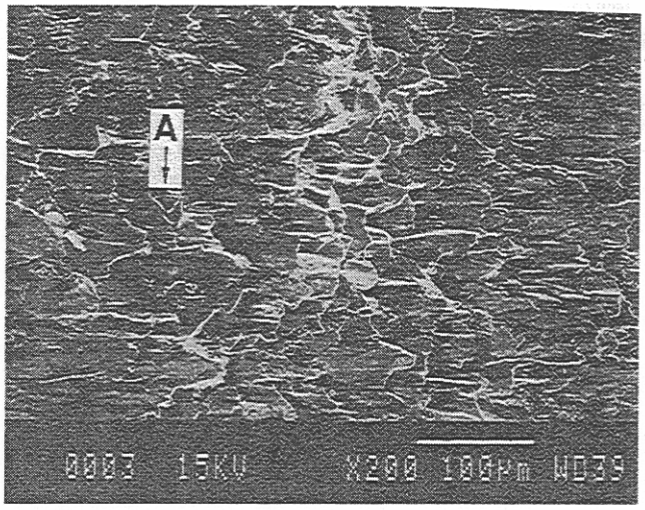


Fig. 7 Fractograph of the shear band surface, $V_0$ = 198 ms$^{-1}$, $\theta$ = 22.9 deg, and $h$ = 79 $\mu$m

appear near the center of the fractograph. These grains are the remaining halves of fractured grains. It is not known whether the fracture surfaces represent certain crystallographic cleavage planes. A combination of ductile rupture of matrix, grain-matrix separations, and grain fracture appears to be responsible for the failure inside the shear band.

**4.3 Role of Material Inhomogeneities in Shear Band Formation.** The deformed microstructure of a tungsten specimen is shown in Fig. 8. This specimen shows intense shear deformation. The material near the top and lower faces experiences less severe shear because the conduction of heat into the flyer and anvil reduces the temperature increases and the amount of thermal softening near the surfaces. No shear band is observed for this material although the impact condition is comparable to those for the WHA specimen in Fig. 5($c$). This result is in contrast to the shear band observed in Fig. 5($c$) for the composite. Similarly, no shear bands were observed in the matrix alloy under similar impact conditions (see Table 1).

The stress-strain curves of pure tungsten, matrix alloy, and the composite obtained from impact experiments are summarized in Fig. 9. Similar stress levels are observed for the tungsten and the composite. The matrix, on the other hand, has lower flow stresses which are approximately one half of those for the tungsten and the composite. Neither the tungsten curve nor the

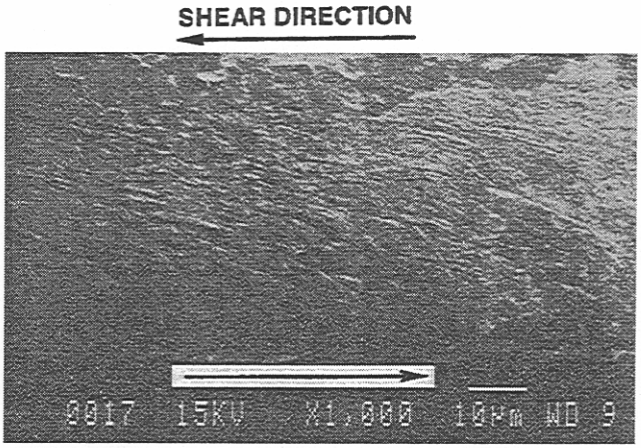


Fig. 8 Deformed microstructure of pure tungsten, $V_0$ = 198 ms$^{-1}$, $\theta$ = 22.9 deg, and $h$ = 91 $\mu$m, sheared for 2 $\mu$s

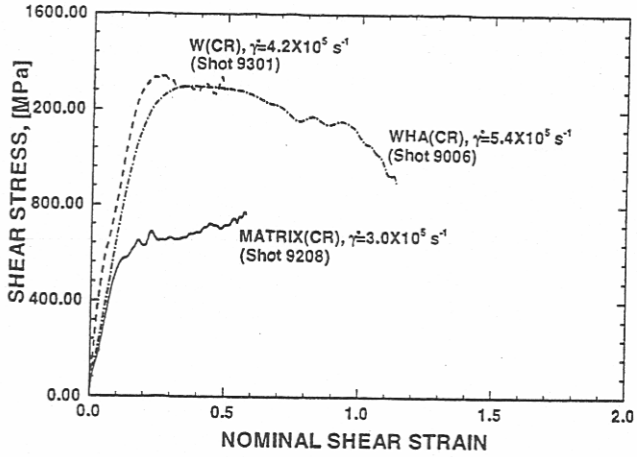


Fig. 9 Dynamic shear stress-strain curves of WHA, pure tungsten, and matrix alloy obtained from pressure-shear plate impact

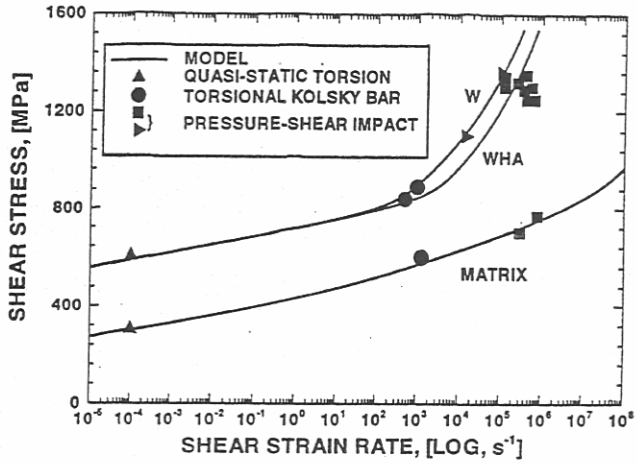


Fig. 11 Strain-rate sensitivities of WHA, pure tungsten, and matrix alloy

matrix curve shows a sharp downturn that indicates the loss of stress-carrying capability associated with the onset of localized deformation. The matrix shows strong strain hardening throughout the deformation. These curves, along with the results of microscopic examinations, suggest that material inhomogeneities inherit in the composite microstructure of WHA enhance the tendency for localization. The heterogeneous material distribution provides conditions under which nonuniform deformation develops more easily. This nonuniformity in turn expedites the initiation of shear bands in the composite, causing the composite to be more susceptible to shear localization than either of its constituent phases when they are tested separately. Numerical simulations of the pressure-shear impact experiments carried out in Zhou et al. (1994) showed that the material inhomogeneities inherit in the composite microstructure indeed dominate the course of shear band formation in WHA. The calculations also confirmed that the two constituent phases are more resistant to shear banding than the composite WHA.

Torsional Kolsky bar and quasistatic torsion experiments conducted on the matrix alloy demonstrate that deformation is essentially uniform in the specimen and no localization is observed. This result is in contrast to the observation of shear band formation in WHA in torsional Kolsky bar experiments reported by Andrews et al. (1992). These results are consistent with the results of pressure-shear plate impact, confirming the higher susceptibility to shear banding of the composite. Torsional experiments on pure tungsten were not successful due to its brittle response. The specimen fractured immediately upon loading. Substantial plastic deformation is achieved in pure tungsten only during pressure-shear plate impact. The presence of pressure is necessary to facilitate plastic deformation in brittle tungsten.

**4.4 Material Response Characterization.** Figure 10 summaries the stress-strain curves for the matrix alloy obtained from quasi-static torsion, torsional Kolsky bar and pressure-shear plate impact. Unlike the composite, the matrix alloy shows strain hardening under both quasistatic and dynamic conditions. This lack of strain softening can be explained as follows. The matrix alloy has a specific heat three times that of the WHA. Its flow stress and density are only approximately one half of those of the WHA. For the same amount of plastic strain, the temperature change would likely be only one third of that for the composite. In addition, the FCC lattice structure of the matrix gives it a higher rate of strain hardening due to its larger number of slip systems and the resulting higher rate of dislocation entanglement. In contract, pure tungsten has a BCC lattice structure and a relatively lower rate of strain hardening.

The strain-rate sensitivities of the WHA, the tungsten and the matrix alloy are shown in Fig. 11. The flow stresses plotted correspond to a shear strain of 0.45. It is noted that the matrix alloy exhibits a relatively weaker strain-rate dependence of flow stress at strain rates above $10^3$ s$^{-1}$. The composite, on the other hand, shows a strong strain-rate sensitivity at high strain rates. The flow stress levels of pure tungsten are slightly higher than those of the composite.

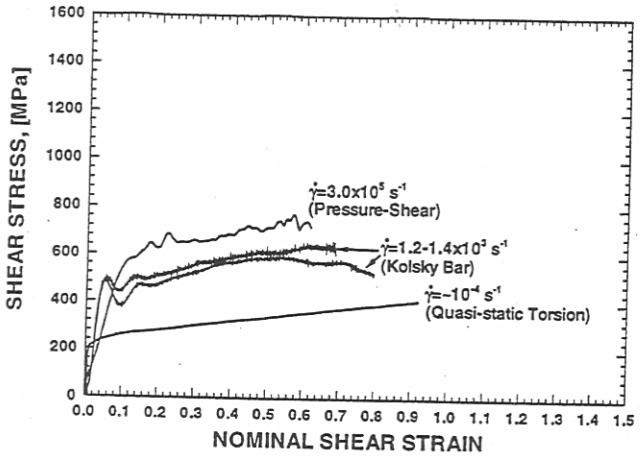


Fig. 10 Shear stress-strain curves of matrix alloy obtained from pressure-shear plate impact, torsional Kolsky bar, and quasi-static torsion

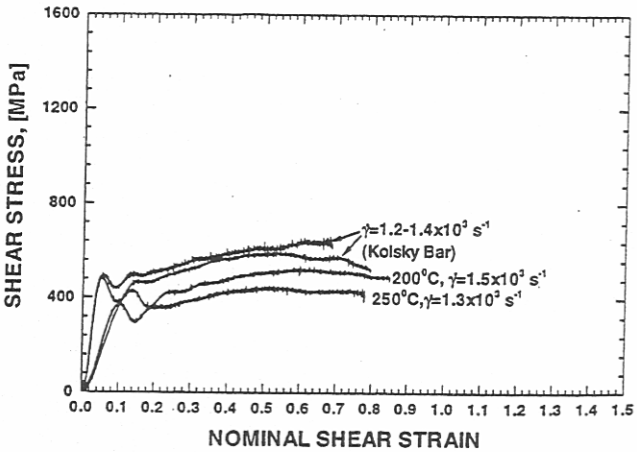


Fig. 12 Shear stress-strain curves of matrix alloy at room temperature, 200°C, and 250°C obtained from torsional Kolsky bar

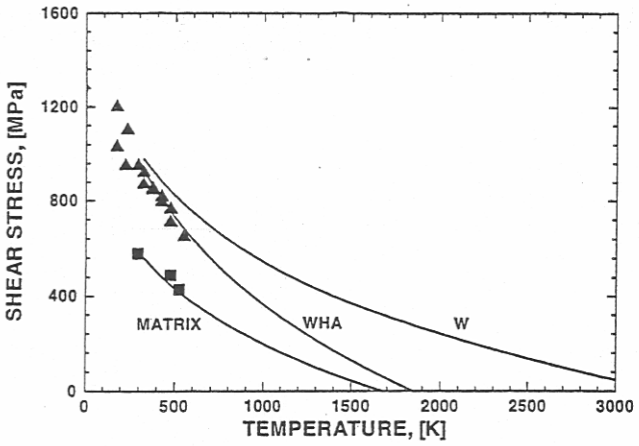


**Fig. 13 Temperature dependence of flow stress for WHA, W, and matrix alloy**

Figure 12 shows the shear stress-strain curves of the matrix alloy obtained from torsional Kolsky bar experiments at room temperature, 200°C and 250°C. Significant thermal softening is seen in this temperature range. The temperature dependence of flow stresses for the composite, pure tungsten, and the matrix alloy are summarized in Fig. 13. The data for WHA are reported by Andrews et al. (1992), Bose et al. (1988), and O'Donnell et al. (1990). Based on the data presented here, Zhou et al. (1994) used a characterization which accounts for viscoplasticity, strain hardening, and thermal softening for the responses of the tungsten and the matrix. This model characterization is indicated by the solid lines. There is a lack of data at high temperatures for all the materials studied. It is assumed that the materials lose all stress-carrying capabilities when the temperature reaches their corresponding melting points. Tungsten shows a much lower rate of thermal softening than the matrix partly because of its high melting temperature (approximately 3300 K versus 1750 K). Simulations of the pressure-shear plate impact experiments on WHA using this characterization of the constituents gave good predictions for the behavior of WHA.

## 5 Conclusions

1 The formation of shear bands in a tungsten heavy alloy is studied using pressure-shear plate impact. In the experiment, the material is subjected to simple shear at shear strain rates up to $7 \times 10^5\ s^{-1}$. The experiment provides an opportunity to relate the shear band development to stress-strain profiles. Dynamic stress-strain relations obtained from the pressure-shear plate impact and torsional Kolsky bar experiments show that the alloy exhibits significant rate sensitivity and thermal softening due to plastic dissipation. Shear bands form when the plastic strain becomes sufficiently large. Significantly more intensely formed shear bands are observed in the pressure-shear impact experiments than those reported for torsional Kolsky bar experiments. The critical shear strain for shear band development is approximately 1–1.5 or 6–8 times that obtained in torsional Kolsky bar experiments.

2 Failure inside the shear bands during pressure-shear impact is a combination of grain-matrix separation, ductile matrix rupture, and grain fracture. Grain-matrix separation seems to be the dominant mechanism through which material failure occurs.

3 Impact experiments show that the flow strength of the WHA follows closely that of the tungsten grains. The matrix has a flow strength approximately one-half that of the WHA. Pure tungsten and the composite show stronger rate sensitivities than the matrix. Pure tungsten and WHA also show thermal softening during pressure-shear impact experiments while the matrix exhibits strain hardening for strain rates up to $3.0 \times 10^5\ s^{-1}$.

4 The presence of different phases serves as a perturbation to deformation that enhances the initiation and development of shear bands. The composite microstructure causes the WHA to be more susceptible to shear banding than either of its constituents when tested separately.

## Acknowledgment

This research was supported by the Army Research Office. Completion of the work was supported by the Office of Naval Research through grant N00014-96-1-1195 to Georgia Tech. We would like to thank Drs. T. W. Penrice and Steven Caldwell of Teledyne Firth Sterling for supplying the cross-rolled tungsten heavy alloy and matrix alloy, and Mr. Meinrad Ostermann of Teledyne Wah Chang for supplying the cross-rolled pure tungsten used in this investigation.

## References

Andrews, E. W., Bower, A. F., and Duffy, J., 1992, "Shear Band Formation in a Tungsten Heavy Alloy," *Proc. Symposium on Shear Bands and Viscoplastic Theories, The 29th Annual Technical Meeting of the Society for Engineering Science,* Sep. 14–16, La Jolla, CA.

Baek, W. H., Hong, M.-H., Lee, S., and Chung, D.-T., 1994, "A Study of the Shear Localization Behavior of Tungsten Heavy Alloys," *Proc. of the 2nd International Conference on Tungsten and Refractory Metals,* A. Bose and R. Dowding, eds., Mclean, VA, pp. 463–471.

Belk, J. A., Waltson, C. H., Bentley, A. R., and Hogwood, M. C., 1994, "Dynamic Deformation Characteristics of Tungsten Alloys," *Proc. of the 2nd International Conference on Tungsten and Refractory Metals,* A. Bose and R. Dowding, eds., Mclean, VA, pp. 389–399.

Bose, A., Sims, D., and German, R. M., 1988, "Test Temperature and Strain Rate Effects on the Properties of a Tungsten Heavy Alloy," *Metallurgical Transactions A,* Vol. 19A, pp. 487–494.

Churn, K.-S., and German, R. M., 1984, "Fracture Behavior of W-Ni-Fe Heavy Alloys," *Metallurgical Transactions A,* Vol. 15A, pp. 331–338.

Clifton, R. J., and Klopp, R. W., 1985 "Pressure-Shear Plate Impact Testing," *Metals Handbook,* Vol. 8, 9th ed., Amer. Soc. Metals, pp. 230–239.

Coates, R. S., and Ramesh, K. T., 1990a, "The Rate-Dependent Deformation of a Tungsten Heavy Alloy," The Johns Hopkins University Report, No. DIL-9001, June, Baltimore, MD.

Coates, R. S., and Ramesh, K. T., 1990b, "The Deformation of Tungsten Alloys at High Strain Rates," The Johns Hopkins University Report, No. DIL-9002, Nov., Baltimore, MD.

Costin, L. S., Crisman, E. E., Hawley, R. H., and Duffy, J., 1979, "On the Localization of Plastic Flow in Mild Steel Tubes under Dynamic Torsional Loading," *Proc. 2nd Conf. on Mech. Properties of Materials at High Rates of Strain,* J. Harding, ed., The Institute of Physics, London, pp. 90–100.

Duffy, J., Campbell, J. D., and Hawley, R. H., 1971, "On the Use of a Torsional Split-Hopkinson Bar to Study Rate Effects in 1100-0 Aluminum," ASME JOURNAL OF APPLIED MECHANICS, Vol. 38, pp. 83–91.

Ekbom, L., 1981, "Microstructural Study of the Deformation and Fracture Behavior of a Sintered Tungsten-Base Composite," *Modern Developments in Powder Metallurgy,* Vol. 14, H. H. Hausner, H. W. Antes, and G. D. Smith, eds., Metal Powder Industries Federation, Princeton, NJ, pp. 177–188.

Hartley, K. A., Duffy, J., and Hawley, R. H., 1985, The Torsional Kolsky (Split-Hopkinson) Bar, *Metals Handbook,* Vol. 8, ASM, pp. 218–228.

Hofmann, H., and Petzow, G., 1984, "Influence of Sintering Atmosphere on Mechanical Properties of Tungsten Based Heavy Alloys," *Modern Developments in Powder Metallurgy,* Vol. 17, pp. 17–31.

Krock, R. H., and Shepard, L. A., 1963, "Mechanical Behavior of the Two-Phase Composite, Tungsten-Nickel-Iron," *Transactions of The Metallurgical Society of AIME,* Vol. 227, pp. 1127–1134.

Krock, R. H., 1964, "Effect of Composition and Temperature on the Dynamic Elastic Moduli of W-Ni-Fe Composite Materials," *Proc. ASTM,* Vol. 64, pp. 712–718.

Kumar, P., and Clifton, R. J., 1976, Optical Alignment of Impact Faces for Plate Impact Experiments. *J. Appl. Phy.,* Vol. 48, No. 3, pp. 1366–1367.

Lassila, D. H., and Connor, A., 1991, "Fracture Behavior of Warm Forged and CVD Tungsten," Lawrence Livermore National Laboratory Report, No. UCRL-JC-106552, *Proc. of the Symposium Tungsten Heavy Alloys—Recent Advances,* TMS/AIME Refractory Metals Committee, TMS/AIME 1991 Annual Meeting, New Orleans, LA.

Magness, L. S., 1992, "Properties and Performance of KE Penetrator Materials," *Proceedings of the First International Conference on Tungsten and Tungsten Alloys,* A. Bose and R. J. Dowding, eds., Nov. 15–18, Arlington VA, Metal Powder Industries Federation, pp. 15–22.

Meyer, L. W., Kunze, H.-D., and Staskewitsch, E., 1983, "Dynamic Strength and Ductility of a Tungsten-Alloy for KE-Penetrators in Swaged and Unswaged Condition under Various Loading," *Proc. 7th International Symposium on Ballistics,* The Hague, pp. 289–293.

Molinari, A., and Clifton, R. J., 1987, "Analytical Characterization of Shear Localization in Thermoviscoplastic Materials," ASME JOURNAL OF APPLIED MECHANICS, Vol. 54, pp. 806–812.

O'Donnell. R. G., and Woodward, R. L., 1990, "The Composition and Temperature Dependence of the Mechanical Properties of Tungsten Alloys," *Metallurgical Transactions A,* Vol. 21A, pp. 744–748.

Rabin, B. H., and German, R. M., 1988, "Microstructure Effects on Tensile Properties of Tungsten-Nickel-Iron Composites," *Metallurgical Transactions A,* Vol. 19A, pp. 1523–1532.

Ramesh, K. T., and Coates, R. S., 1992, "Microstructural Influences on the Dynamic Response of Tungsten Heavy Alloys," *Metallurgical Transactions A,* Vol. 23A, pp. 2625–2630.

Tham, R. H., and Hohler, V., 1995, "Dynamic Behavior of Novel Tungsten Penetrator Materials," *Proc. of the 3rd International Conference on Tungsten and Refractory Metals,* A. Bose and R. Dowding, eds., Mclean, VA, pp. 159–166.

Yadav, Y., and Ramesh, K. T., 1995, "The Mechanical Properties of Tungsten-based Composites at Very High Strain Rates," *Materials Science and Engineering,* Vol. A203, pp. 140–153.

Weerasooriya, T., 1994, "Effect of Sudden Change in Strain Rate on the Deformation and Failure Behavior of a Tungsten Heavy Alloy," *Proc. of the 2nd International Conference on Tungsten and Refractory Metals,* A. Bose and R. Dowding, eds., Mclean, VA, pp. 455–471.

Weerasooriya, T., Beaulieu, P. A., and Swanson, R., 1992, "Deformation and Failure Behavior of 93W-5Ni-2Fe at High Strain Rate Shear Loading," U.S. Army Materials Technology Laboratory Report, No. MTL TR 92-19, Watertown, MA.

Weerasooriya, Moy, P., and Dowding R. J., 1994, "Effect of W-W grain Contiguity on the High Shear Strain Rate Behavior of 93W-5Ni-2Fe Tungsten Heavy Alloy," *Proc. of the 2nd International Conference on Tungsten and Refractory Metals,* A. Bose and R. Dowding, eds., Mclean, VA, 401–409.

Woodward, R. L., Alkemade, S. J., and Magness, L. S., 1994, "Strain Localization and Fracture in Dynamic Dumbbell Compression of Tungsten Alloys," *Proc. of the 2nd International Conference on Tungsten and Refractory Metals,* A. Bose and R. Dowding, eds., Mclean, VA, pp. 431–445.

Woodward, R. L., Baldwin, N. J., Burch, I., and Baxter, B. J., 1985, "Effect of Strain Rate on the Flow Stress of Three Liquid Phase Sintered Tungsten Alloys," *Metallurgical Transactions A.* Vol. 16A, pp. 2031–2037.

Zhao, D., Valencia, J. J., and McCabe, T. J., 1995, "Mechanical and Microstructural Behavior of Tungsten Alloys during High Rate Deformation," *Proc. of the 3rd International Conference on Tungsten and Refractory Metals,* A. Bose and R. Dowding, eds., Mclean, VA, pp. 123–130.

Zhou, M., Needleman, A., and Clifton, R. J., 1994, "Finite Element Simulations of Dynamic Shear Localization," *Journal of Mechanics and Physics of Solids,* Vol. 42, No. 3, pp. 423–458.

Zurek, A. K., and Follansbee, P. S., 1995, "A Comparison of Shear Localization Susceptibility in U-0.75 Wt Pct Ti and W-Ni-Fe during High Strain Rate Deformation," *Metallurgical and Materials Transactions A,* Vol. 26A, pp. 1483–1490.